MrLavaLoba: a new probabilistic model for the simulation of lava flows as a *settling* process

Mattia de' Michieli Vitturi and Simone Tarquini, Istituto Nazionale di Geofisica e Vulcanologia, Pisa, Italy

Abstract

A new code to simulate lava flow spread, MrLavaLoba, is presented. In the code, erupted lava is itemized in parcels having an elliptical shape and prescribed volume. New parcels bud from existing ones according to a probabilistic law influenced by the local steepest slope direction and by tunable input settings. MrLavaLoba must be accounted among the probabilistic codes for the simulation of lava flows, because it is not intended to mimic the actual process of flowing, but rather to guess the most probable inundated area and thickness. The code does not provide directly the progression with time of a flow field. The code's flexibility allows it to produce variable lava flow spread and emplacement according to different dynamics (e.g. pahoehoe or channelized-'a'ā). The code does not directly provide the progression of a flow field with time. For a given scenario, it is shown that model outputs converge, in probabilistic terms, towards a single solution. The code is finally applied and compared to real cases in Hawaii and Mt Etna, and the obtained maps are shown.

The model is written in Python and the source code is available at http://demichie.github.io/MrLavaLoba/.

1. Introduction

Forecasting lava flow emplacement is a critical issue at many basaltic volcanoes where the propagation of flowing lavas threaten surrounding properties and infrastructures. Lava flow simulation is becoming an important tool for hazard and risk assessment before and during ongoing eruptions (Favalli et al., 2009a, 2009b; Cappello et al., 2016; Cordonnier et al., 2016; Richter et al., 2016; Dietterich et al., 2017).

Existing numerical codes for the simulation of lava flow emplacement are either so-called deterministic codes based on the solution of some

simplification of the physical governing equations of this phenomenon (Hidaka et al. 2005; Del Negro et al. 2008; Crisci et al. 2010), or, instead, so-called *probabilistic codes* based on the simple evidence that lava flows tend to follow the steepest descent path downhill (Macedonio et al. 1990, Felpeto et al. 2001; Favalli et al. 2005). Deterministic codes attempt to mimic, with a sufficiently accurate approximation, the thermo- and/or fluid-dynamics of the natural system, so that the emplacement of the erupted volume over time can be derived as a single solution if input parameters are set to the correct values. Probabilistic codes instead give more emphasis to the uncertain character of the solution (Gilbert and Sparks 1998) because the parameters and the processes under examination are known only imprecisely (e.g. with respect to the effusion rate, Harris et al. 2007).

Deterministic simulations, in principle, provide a final coverage and thickness of lava flow field as well as detailed information of the lava flow emplacement over time, including the velocity of advancement of the front and the overall shape and thickness of the final flow field (Vicari et al. 2011). The output of a probabilistic simulation typically provides the most likely path of the flow and the associated inundated area, without constrain on the thickness of the final flow field nor temporal insight into the planimetric evolution of the lava flow (Tarquini and Favalli 2011, 2013, 2016; Mossoux et al., 2016).

Glaze and Baloga (2013) recently developed and Hamilton et al. (2013) tested a new code which was specifically focused on the simulation of late-stage pahoehoe lobes where random processes dominate emplacement (Baloga and Glaze 2003; Glaze and Baloga 2013). This code can be considered probabilistic because the approach for selecting the transfer direction (North, South, East or West) is based on the generation of a random number. In contrast with earlier probabilistic codes, this code can provide as output the volume of the emplaced lava over time (i.e. the supply rate). This approach utilizes erupted volumes, one of the most critical input parameters considered by deterministic codes, within the stochastic approach of probabilistic codes. This allows for properties of the lava field, such as final thickness, to be addressed through a probabilistic approach.

In this paper, a new probabilistic code to simulate lava flows is presented. This code, named *MrLavaLoba*, rests on an approach similar to the one introduced by Glaze and Baloga (2013). Substantial differences are introduced, such as taking into account the topography and removing the limitation of only four transport directions allowed. We tested MrLavaLoba for the simulation of the emplacement of pahoehoe and channel-fed ‘a‘ā lava flows, and we show that, through the tuning of input parameters, the model can provide solutions for coverage area and thickness.

2. Growth and thickening of basaltic lava flows

The emplacement of basaltic lava flows can occur according to substantially different dynamics, ranging from pahoehoe lobes, which can later evolve into very thick sheet flows through progressive inflation (Hon et al., 1994; Self et al., 1998; Hoblitt et al., 2012), to the massive advancement of ‘a‘ā or blocky flows (Kilburn 2000), which usually progress as large channelized flows (Guest et al., 1987; Lipman and Banks 1987; Harris et al., 2002; Tarquini et al., 2012a; Wadge et al., 2012; Wantim et al., 2013).

Although they show different dynamics and growth mechanisms, both small pahoehoe lobes and large channelized flows tend to create a thickening deposit over time (Tarquini 2017), which is as to say that, after being transported for a given time, lava parcels become part of a static deposit. As a rule of thumb, single lobes thicken as a result of injection of lava beneath a thickening crust, i.e. through an endogenous growth (Jurado-Chichay and Rowland 1995; Kauahikaua et al., 1998; Thordarson and Self 1998; Walker 1991, 2009). In contrast, individual open channels usually thicken through an iterative stacking process, i.e. according to a surface-fed growth mechanism (Sparks et al. 1976; James et al. 2007, 2012; Glaze et al. 2009; Applegarth et al. 2010a; Tarquini and de’ Michieli Vitturi 2014).

The thickening of individual flow units (*sensu* Walker 1971) is not the only mechanism which increases the overall lava deposit thickness. The formation of

multiple flow units also influences the overall thickness (Guest et al. 1987; Kilburn and Lopes 1991). New flow units can substitute or accompany former ones, flowing at their sides or on top of them, producing a compound flow field (Walker 1971, 1973; Wadge 1978; Kilburn and Lopes 1988; Applegarth et al., 2010b). The typical shorter runout of the active flow units during the waning phase of basaltic eruptions (due to a decreasing supply, Wadge 1981), further promotes the piling up of late flow units over the earlier ones (Guest et al. 1987; Applegarth et al. 2010a; James et al., 2009; Tarquini 2017).

In summary, although spreading and lengthening are also very important, the emplacement of basaltic lava flows is always characterized by a progressive thickening. As a rule, an increasing thickness of the lava flow field means an increasing thickness of the solid portion (essentially a static lava deposit - Figure 1), while the amount of liquid, hot lava transported downhill tends to decrease with time as the lava supply decreases (Tarquini 2017).

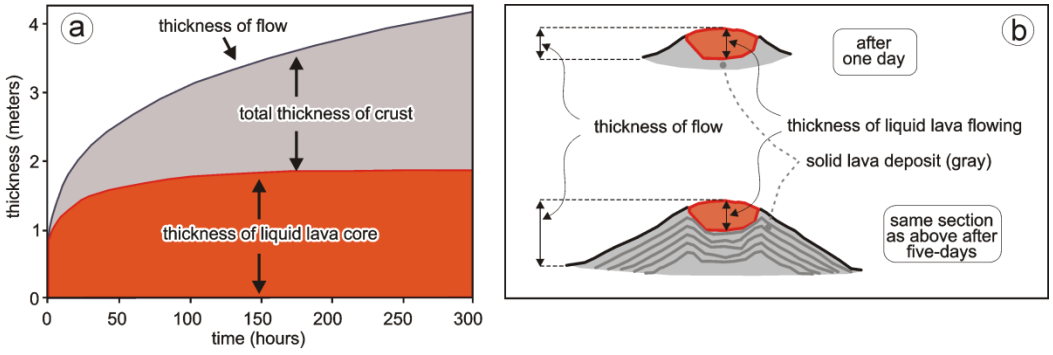

Figure 1. Thickening of basaltic lava flows through time. (a) Simplified progression of the inflation process of a sheet flow in Hawaii (13 April 1990) based on measurements and modeling presented by Hon et al. (1994). (b) Transect section showing the progressive stacking of lava blankets incrising the total height of a lava channel measured at Mt Etna (Italy) from a Lidar survey carried out during the early phase of the 2004-2005 eruption (modified after Tarquini and de' Michieli Vitturi 2014). Static lava deposit is gray in figure, molten lava is orange.

As a result, the progressive growth of a lava flow can be viewed as a process through which the supplied lava is settled to a given, permanent position located downhill from the vent, and the transport process (the actively flowing lava), determines the path along which lava parcels are settled (Harris and Rowland 2001; Wright et al., 2008).

Parcels are not settled only at the flow front (Borgia et al. 1983; Young and Wadge 1990; Castruccio et al., 2014), but also behind it, where batches of lava are settled along extensive sectors of the generic lava flow unit (James et al. 2007; Glaze and Baloga 2006; Baloga and Glaze 2008; Glaze et al., 2009; Favalli et al., 2010). Thus, the lava transport process is closely intermingled with lava settling. This concept is the basis of MrLavaLoba.

3. The code

The main inputs of the code are topography and erupted volume. There are no special requirements as for the resolution of the topography to be used as computational domain, the code was successfully tested using DEMs ranging from 5 to 30 m in resolution. The lava supplied from the vent is itemized in parcels (lobes). The code combines in a single probabilistic procedure two elements: (1) the path followed downhill by the flowing lava, and (2) the settling of lava parcels along the path. A spectrum of tunable parameters determines the progression downhill of the flow (i.e. the extension of the flow path), which is obtained by iteratively positioning new lava parcels in their final, permanent position. In practice, the distribution of lava parcels over the pre-emplacement topography is obtained without tackling directly the complexity of the transport dynamics but through much simpler probabilistic rules: one giving the direction of propagation of new lobes, and one determining where new lobes bud.

The parameters determining the probability distributions of both rules have to be tuned to a given scenario through comparison with selected real lava flows.

159

160 *3.1 The geometry of lava parcels*

161 Lava parcels are represented by elliptical lobes having a constant area and
162 a prescribed thickness (i.e. the volume is fixed). Parcel thickness can be of the
163 order of centimeters down to millimeters. This low thickness of individual
164 parcels is, on its own, not a realistic representation, but the individual parcels
165 pile up to produce realistic lava flow thicknesses. If the volume of erupted lava
166 and the area of a lobe are held constant, as computational lobes beome
167 thinner, the number of lobes becomes greater. The greater the number of
168 lobes, the closer the spreading of the lava to the expectation associated with
169 the probabilistic elements of the code. For example, considering a flat
170 topography, all directions of lava flows have the same probability, so we expect
171 the flow to spread radially. If the entire erupted volume is assigned to a single
172 parcel, only one direction will be represented in the output. In contrast, if the
173 volume is partitioned into a suffiently large number of thin parcels, the
174 spreading will approach a uniform circle with the vents at its center.

175 The geometry of a new elliptical parcel l_i (the lobe) is defined by the
176 eccentricity e_i and by the azimuthal orientation of the major axis of the ellipse
177 az_i''. Lobe position, instead, is defined by the geographic coordinates (x_i,y_i) of
178 the center of the ellipse (c_i) representing the parcel (Figure 2). With the
179 notation just introduced, the equation of the elliptical lobe write as

180 $$\frac{[(x-x_i)cos(az_i'')+(y-y_i)sin(az_i'')]^2}{a_i^2}+\frac{[(x-x_i)sin(az_i'')-(y-y_i)cos(az_i'')]^2}{b_i^2}=1$$

181 with the semimajor a and semiminor axis b satisfying

182 $$e_i=\sqrt{1-\frac{b_i^2}{a_i^2}};\quad \pi a_i b_i = lobe\ area.$$

183

184 The first parcel is set on the vent, and each subsequent parcel buds from
185 the edge of an older parcel (denoted as parent parcel), which has been already
186 set. The point where the new parcel will bud (budding point, b_p) is determined
187 according to the following steps:

188

- STEP 1. A preliminary direction az_i is given by the direction from the center of the parent lobe (c_p) to the point of minimum elevation on the boundary of the elliptical parcel (Figure 2a);
- STEP 2. A random perturbation ε_{az}, with a probability distribution defined as a function of the local slope, is added to az_i resulting in a new preliminary orientation az_i' (Figure 2b).
- STEP 3. An inertial factor accounting for the orientation of the parent lobe (az_p) is considered, resulting in the final orientation $az_i''=f(az_i',az_p)$ (Figure 2c). This final direction from the center of the parent lobe determines the budding point b_p on its boundary.

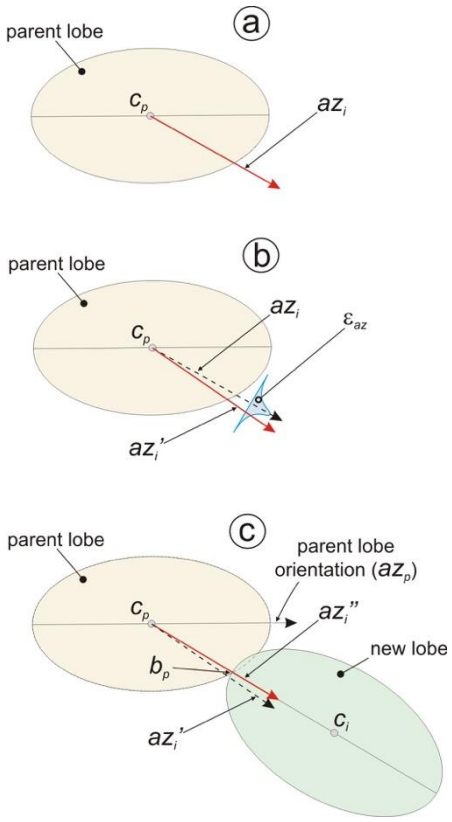

Figure 2. Sketch of the positioning of a new lobe (light green ellipse) with respect to the selected parent lobe (light yellow ellipse). The major axes of both ellipses are plotted. Panels (a) to (c) illustrate the three steps implemented and described in the main text. The relative weight between the three factors (a) to (c) depends on the values selected for the relevant parameters. The budding point b_p always lays on the boundary of the ellipse representing the parent

lobe, and the line joining c_p and b_p identifies the direction of propagation of the flow. The center c_i of the new lobe always lays along this direction az_l'', and is defined by the distance d between c_p and c_i, which can vary between a minimum ($c_i = b_p$) and a maximum (the new ellipse passes through b_p) according to the value set in input to the parameter *dist_fact* within the interval [0;1]. The latter case (*dist_fact* = 1) is illustrated in figure.

The probability distribution of the random perturbation (ε_{az}) introduced in the second step is determined by one of the set input parameters, and is ruled by two additional parameters: (i) the local slope (θ, degrees); and (ii) a dimensionless input parameter α_{max}, which can vary within the interval [0;1]. As stated above, the flatter the topography, the wider the range of possible directions of propagation. Consequently, the steeper the slope in c_p, the lower the probability of having a large perturbation (ε_{az}) and the closer az_i' will be to the preliminary direction (az_i). The probability distribution associated with the perturbation is a truncated normal distribution in the interval [-180;180] (Chopin 2011) with zero as the mean value and with a standard deviation defined by the following equation:

$$s = \frac{(1 - a_{\max})(90 - q)}{a_{\max} q} \qquad (1)$$

When α_{max} = 0°, or when the local slope $\theta = 0$, all perturbations have the same probability, resulting in a random choice of az_l'. When α_{max} > 0, a null perturbation (the maximum slope direction) has a larger probability, and this probability increases with increasing value of α_{max}. If α_{max} = 1 (excluding when $\theta = 0$) no perturbation is added to az_i resulting in a new preliminary orientation $az_i' = az_i$. (i.e. the budding process follows strictly the steepest descent path, making the choice of the budding point purely deterministic). The probability density function for several values of α_{max} and θ are plotted in Figure 3.

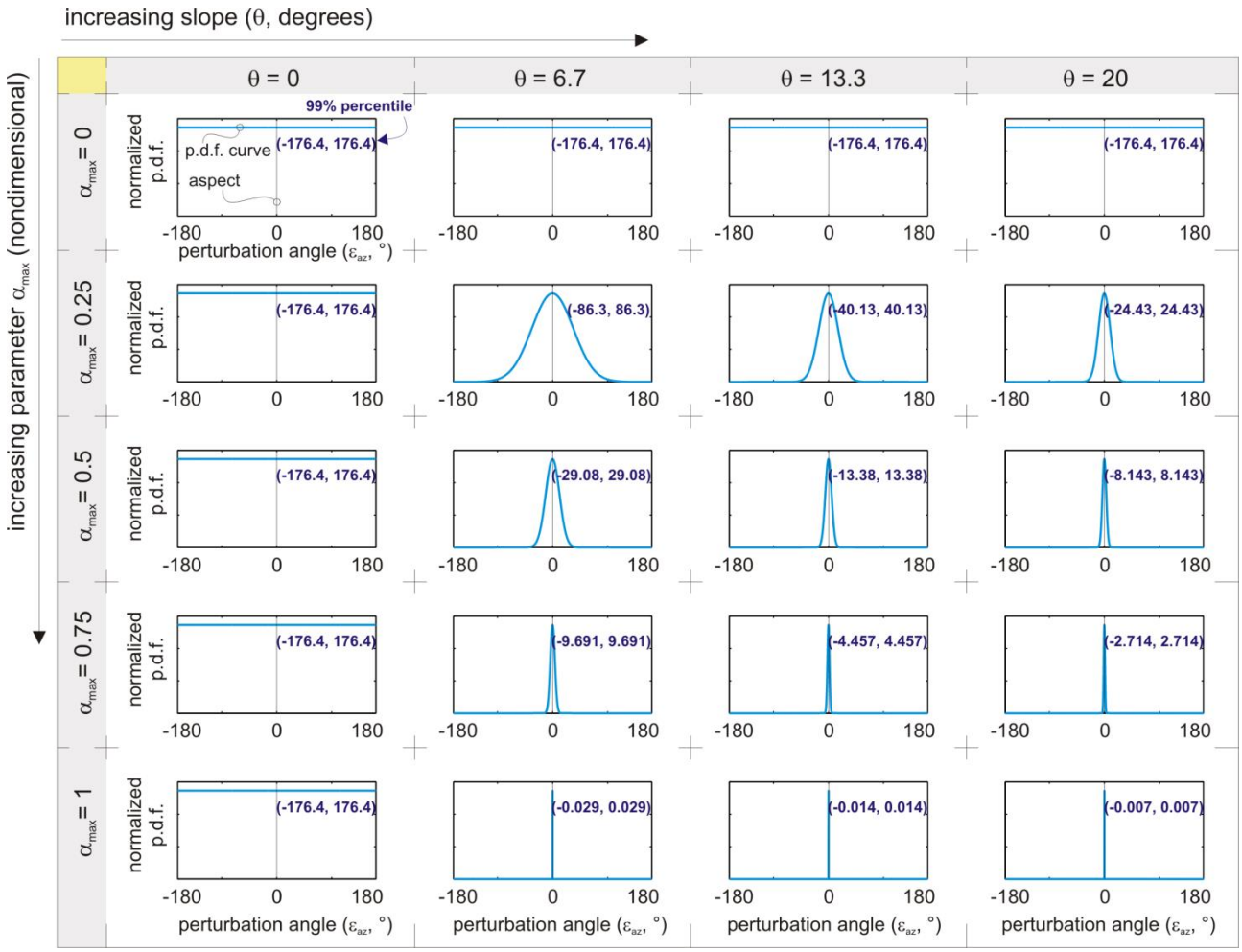

Figure 3. Probability density function (p.d.f.) of the angular perturbation ε_{az} added to the local aspect az_i. When local slope (θ) is null or the input parameter α_{max} = 0, the probability distribution from which ε_{az} is sampled is uniform; as θ and/or α_{max} increase, the probability of large values of ε_{az} decreases, so that az_i' tends to coincide with the local steepest descent.

The inertial contribution is a deterministic function of the slope at c_p (the shallower the slope in c_p the larger the inertial contribution) and of a further input parameter *inertial_exponent* controlling how much the new orientation az_i'' is inherited from the parent lobe. This negative relation between the *inertial_exponent* and slope may sound counterintuitive, but one has to take into account that a higher slope typically promotes flow bifurcation (Dietterich and Cashman 2014), which always result in lateral spreading of the flow field (Tarquini and Favalli 2011; 2016). In contrast, emplacement on shallow slopes

tend to follow a straight path, as seems to have happened during the emplacement of the 180 km long pahoehoe lava flow described by Giacomini et al. (2009) in the almost flat Payen volcanic Complex (Argentina), or as happened during the 2014-2015 Holuhraun eruption (Iceland), when the initial flow (slabby pahoehoe to aha in nature, Pedersen et al., 2017) progressed straight along the steepest path for about 20 km driven by a very low average slope of 0.2 degrees (Tarquini et al., 2015).

Finally, the eccentricity e_i of the budding lobe is defined as a function of the slope from the center of the parent lobe to the budding point b_p, defined as the intersection between the boundary of the parent lobe and the ray from the center of the lobe with direction az_i'' (Figure 2). The steeper the slope the larger the eccentricity, with circular lobes forming over a flat topography. We remark here that while the eccentricity of the lobes changes as a function of the slope, the area and the thickness are fixed (unless otherwise stated in the input settings).

3.2. Budding of parcels

The code proceeds by iteratively setting new parcels on the topography until their total volume equals that prescribed fort the simulation. The first parcel is set on the vent. The second parcel will bud from the first one, which is the only one already set on the topography. From the third parcel onward it is necessary to make a choice to select which will be the parent parcel among all the parcels already positioned. This choice, input parameter *lobe_exponent*, has a critical importance to the propagation of the flow, and is defined with a value within the interval [0;1]. The closer *lobe_exponent* is to 0, the higher the probability that younger lobes will be the parent of a new lobe. If *lobe_exponent* = 0, the youngest lobe will be the parent lobe of the next, and a single chain of lobes trending downhill originates (figure 4a). At the other extreme, when *lobe_exponent* = 1, all existing lobes have the same probability to be the parent, and the code generates more complex features, with frequent overlapping between lobes and widening of the flow through multiple branching (figure 4b). When *lobe_exponent* = 0 (budding from the last lobe), the

user can select a maximum number of lobes constituting a chain, and the creation of a chain will be reiterated several times generating a series of smaller chains (Figure 4c) until the total volume is considered. The latter case mimics the creation of many perturbed steepest descent paths implemented in the DOWNFLOW code (Favalli et al. 2005). The number of parcels forming the chains can be fixed as a constant or as variable within a range, and influences the obtained runout. Several further tuning options are implemented, for example to account for a given propensity to lengthening, widening or thickening of the flow field, and details are provided in the largely commented source code available at the model repository (http://demichie.github.io/MrLavaLoba/).

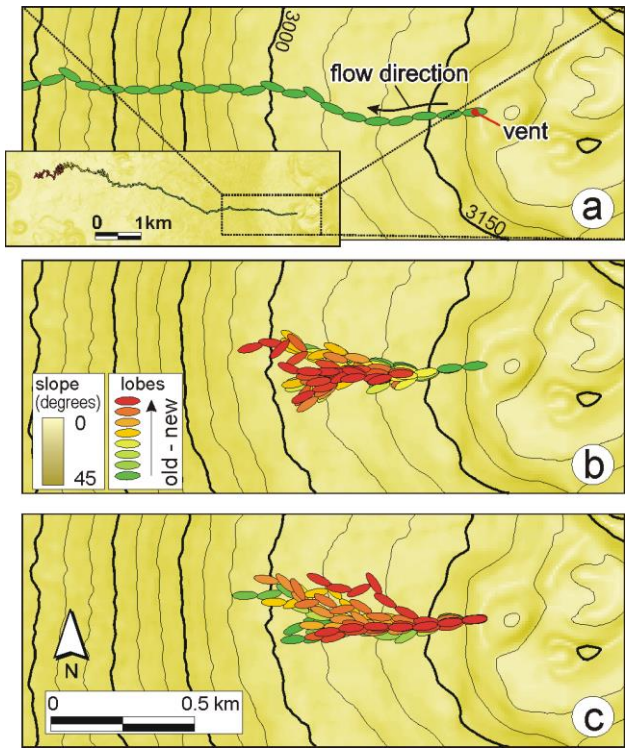

Figure 4. Simplified MrLavaLoba outputs illustrating the result of the budding of 150 parcels (2000 m^2 in area and 0.5 m in thickness each for a cumulative 150 × 10^3 m^3) with different input settings. All the other input parameters remained fixed. (a) shows the output with *lobe_exponent* = 0 (budding is always from the youngest lobe) and without restarts from the vent (all the lobes are visible in

304 the inset); (b) shows the output with *lobe_exponent* = 1 (budding is from a
305 random parent lobe) and without restarts from the vent; (c) shows the output
306 when *lobe_exponent* = 0 as in (a), but with multiple restarts from the vent.
307
308 In addition to being at a given position and possessing a given geometry,
309 each parcel is also assigned with two additional attributes: (i) its distance
310 downflow from the vent, and (ii) its number of descendant parcels. The distance
311 from the vent is an integer value that sums the number of parcels (i.e. the
312 number of budding processes) separating each parcel from the vent. This
313 parameter tracks the length of the path (ideally) followed by each lava parcel to
314 attain its final position, and is computed for each new parcel as the distance
315 value of its parent lobe increased by one. The number of descendants is an
316 integer value, and is updated each time a new parcel is set by adding one to all
317 the ancestor parcels, from the parent lobe backward to the vent. If we assume
318 that a newly generated lobe has travelled from the vent to its actual settling
319 position passing through all ancestor parcel positions, then the number of
320 descendants represents the number of lava parcels that passed through a
321 particular lobe, and this information can be used to describe the relative
322 probability of a given model cell being inundated.
323
324
325 *3.3. The output of a simulation*
326 Once the selected number of parcels has been settled as vector lobes on
327 the topography (Figure 4), this result is processed to derive an output in grid
328 format (Figure 5). For convenience, any output grid has the same cell size and
329 the same extent as the input topography used as computational domain. It is
330 important to stress that, to improve the readability, the lobe and the grid cell in
331 Figure 4 have a rather similar size, but in performing real simulations the lobe
332 should be about 5-10 times bigger than the grid cell in order to optimize the
333 computational time (see also section 3.6).
334 Up to three grids can be saved as output: (i) the grid representing, at each
335 cell, the thickness of the lava deposit, obtained as the cumulative volume of the

portions of the parcels covering each cell divided by the cell area; (ii) the grid representing, at each cell, the sum of descendant parcels for all the parcels touching that cell, indicating the total number of transits in that cell (proportional to the local probability of inundation, or the hazard); and (iii) the grid expressing, at each cell, the minimum along-path distance from the vent among all the parcels covering that cell (indicative of the minimum time required to reach the cell). For the latter grid, the distance is computed as described in the previous section.

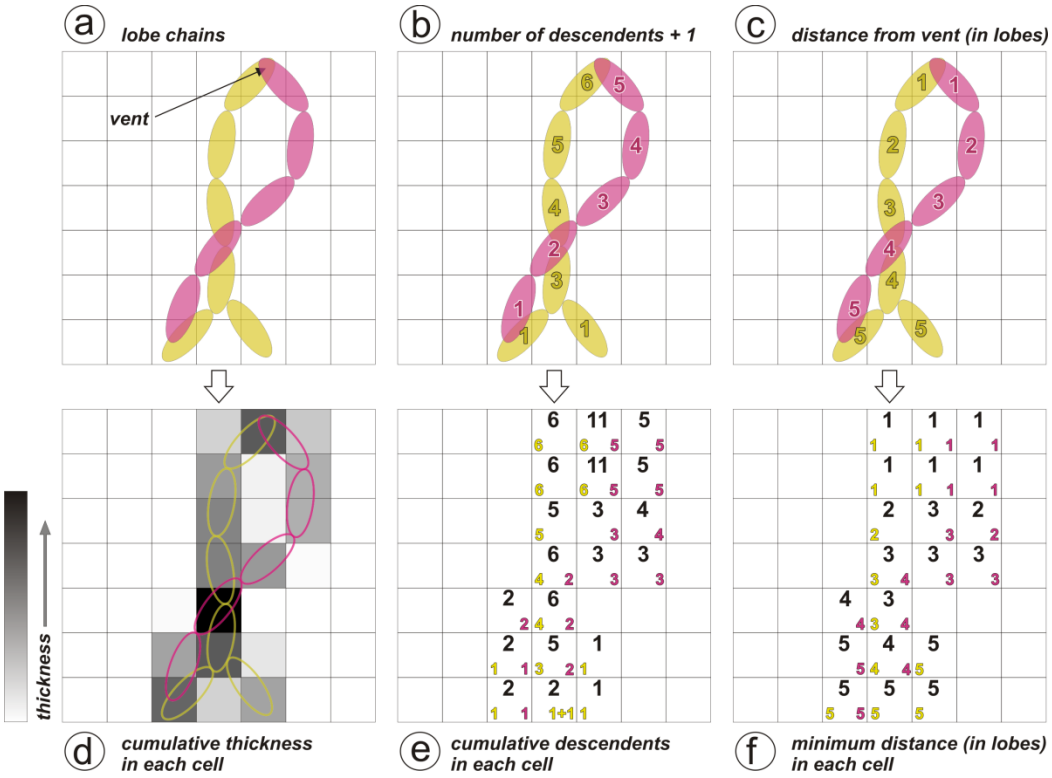

Figure 5. Examples of simulation outputs: from vector (a-c) to raster format (d-f). (a) Two lobe-chains generated from the vent with different budding rules: budding strictly from the last lobe (red chain) or not (yellow chain); (b) each lobe is assigned with the number of descendants (+1); (c) each lobe is assigned with the distance from vent measured as number of lobes (by following backwards the budding process); (d) output grid where the thickness in each cell is assigned according to the portion(s) of the lobe(s) covering it; (e) output grid of the hazard in which each cell is assigned with the sum of the descendants (black number) of all the touching lobes (discarding direct buddying); (f) output grid of the minimum distance from the vent.

The code allows for saving *masked* grids obtained by considering only some of the inundated (or touched) cells. This option is controlled by the input parameter *masking_threshold*, expressed in fraction of the total volume (i.e. varying within the interval [0; 1]). As an example, if *masking_threshold* is set to 0.95 for the thickness grid, the thinnest portion of the final lava deposit representing 5% of the total volume emplaced is filtered from the results (see Figure 6 and compare maps in the first and second rows). When the masking is applied to the hazard grid, the threshold function removes 5% of the total volume emplaced in the areas with the lowest probability of being inundated. The masking threshold is fundamental for the definition of convergence of the outputs of the code, as described in the next section.

3.4. The convergence of simulations

MrLavaLoba is a probabilistic model, and repeated runs always yield different results even if input parameters are unchanged. If this uncertainty is not assessed, the latter point can undermine the reliability of a simulation. For a fixed total emplaced volume and input settings, reducing the thickness of lava parcels means an increase in the total number of parcels, and hence an increase in the statistical meaningfulness of the lava spreading process. For each model realization, the local thickness (i.e. the number of parcels over a cell) can be seen as the probability of a point of the topography to be inundated. We have found that using a sufficiently high number of parcels, for a fixed cumulative volume, fixed input settings and a fixed threshold (*masking_threshold*), the masked area of inundation, obtained by removing the low probability tails of the deposit, converges to a univocal high probability region. We do not find a convergence using the complete unfiltered results. The convergence of the masked result demonstrates the dependability of the simulation output.

The convergence can be tested by iterating the following procedure a number, N, of times. In the first iteration (i.e. $i = 0$), considering a fixed cumulative volume of lava, a fixed number of lava parcels and fixed input settings, the simulation is repeated twice, producing two output grids, which are then masked (e.g. by setting *masking_threshold* = 0.95) obtaining the two

grids G_{i_1} and G_{i_2}. We denote with C_{i_1} and C_{i_2} the area covered by the masked grids, and we define the coverage convergence index μ_i (quantifying the similarity between the two masked results) as follows:

$$\mu_i = \frac{C_{i\_1} \bigcap C_{i\_2}}{C_{i\_1} \bigcup C_{i\_2}} \quad (2)$$

At each new iteration (i.e. i = 1, 2, 3 .. N), the number of parcels is multiplied by a given factor (here set to 2), while the thickness of parcels is divided by the same factor (all the other setting remaining fixed), thus keeping constant the cumulative volume. By applying equation (2) at each iteration, a series of coverage convergence indexes is obtained (μ_1, μ_2.. μ_N). If the obtained sequence tends to 1, then the masked inundated area converges towards a univocal solution.

In order to illustrate the convergence, we carried out a series of tests with a cumulative 150 × 10^3 m^3 bulk volume on the Etna topography. For the first iteration of the convergence test, 150 lobes (2000 m^2 in area each as in Figure 4) are used, resulting in a constant thickness of 0.5 m for each lobe. In the second iteration the number of lobes is doubled, with 300 parcels having constant thickness of 0.25 m, and so on up to the 11th iteration when 156 300 lobes approximately 0.5 mm thick are considered for the settling process. Figure 6 shows graphically a few examples of the iterative computation of the coverage convergence index for α_{max} = 0.9 and *lobe_exponent* = 0.6, highlighting the convergence of the masked output to a univocal area (thus implying that μ_i tends to 1 as the number of iteration of the procedure increases). Figure 7a-b further illustrates that MrLavaLoba simulation outputs converge toward a unique solution as the number of parcels increases for a suite of combinations of different values for input parameters. The convergence of μ_i to 1 is not monotonic because the model is probabilistic.

In parallel with the convergence of the coverage convergence index μ_i we also checked the convergence of the thickness of the masked deposit (i.e. G_{i_1} and G_{i_2} defined above) by verifying that the discrepancy between the two

outputs obtained at each iteration (defined below by the additional thickness convergence index τ_i) vanishes to zero as the number of iterations increases (Figure 7c-d):

$$\tau_i = \frac{V_d}{\max(V_{i\_1}, V_{i\_2})} \quad (3)$$

where $V_d = \int_{C_{i\_1} \cap C_{i\_2}} abs(G_{i\_1} - G_{i\_2})$, $V_{i\_1} = \int_{C_{i\_1} \cap C_{i\_2}} G_{i\_1}$ and $V_{i\_2} = \int_{C_{i\_1} \cap C_{i\_2}} G_{i\_2}$. For an increasing number of iterations *i*, if τ_i tends to zero (as in Figure 7c-d), then the output of the simulation tends to an univocal solution (i.e. a given grid of the thickness). The performed tests also indicate that for a number of iterations close to 10^3, the obtained results appear to converge, as shown by the trends in the plots of both convergence indexes (Figure 7).

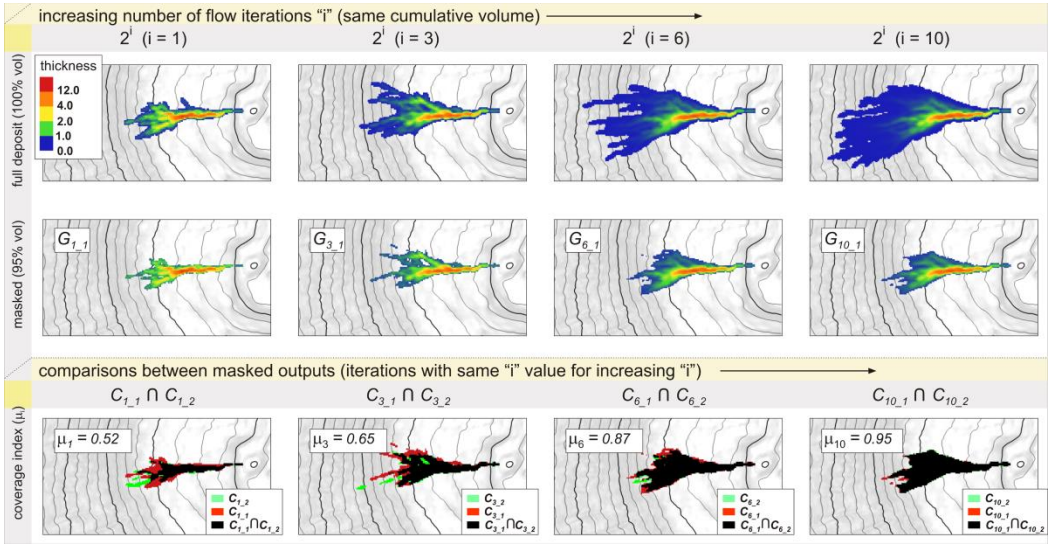

Figure 6. Convergence of the outputs of MrLavaLoba simulations. First row: unmasked outputs of simulations (thickness grid) obtained with an increasing number of parcels. Second row: same as above, but with masked outputs (*masking_threshold* = 0.95). Third row: intersections between coverage of the masked outputs to compute μ_i.

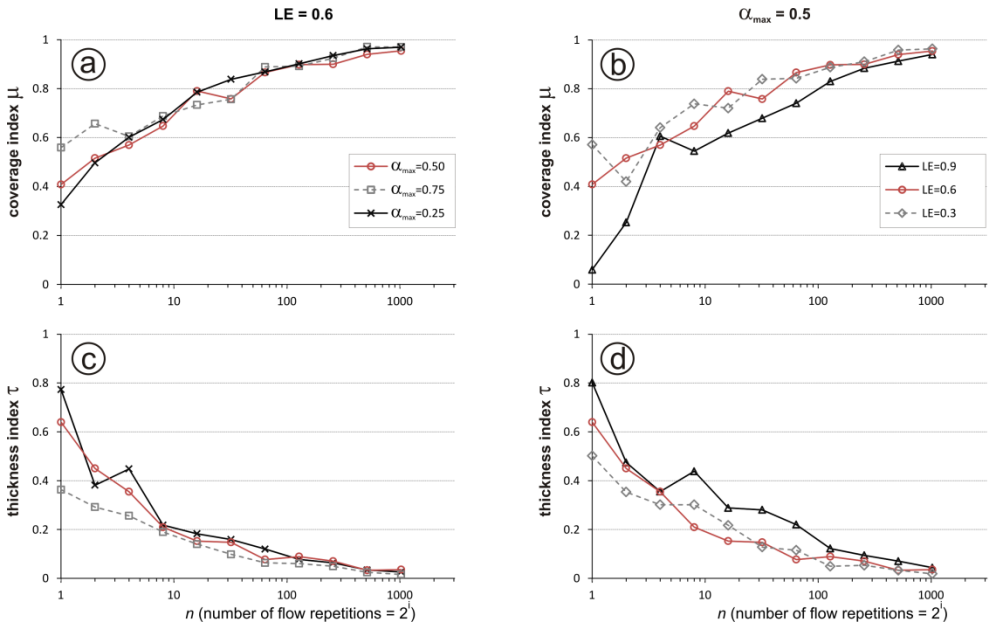

Figure 7. Convergence of the coverage and thickness of the masked grids for different values of *lobe_exponent* (LE) and α_{max}. The coverage convergence index μ_i tends to 1 (a-b) and thickness convergence index τ_i tends to 0 (c-d) as the number of iterations increases. The obtained plots support that the simulations always converge towards a unique result.

In order to explore graphically how the convergence solution varies according to different input settings, the grids of the thickness obtained in performing the convergence test for varying input parameters are shown in Figure 8.

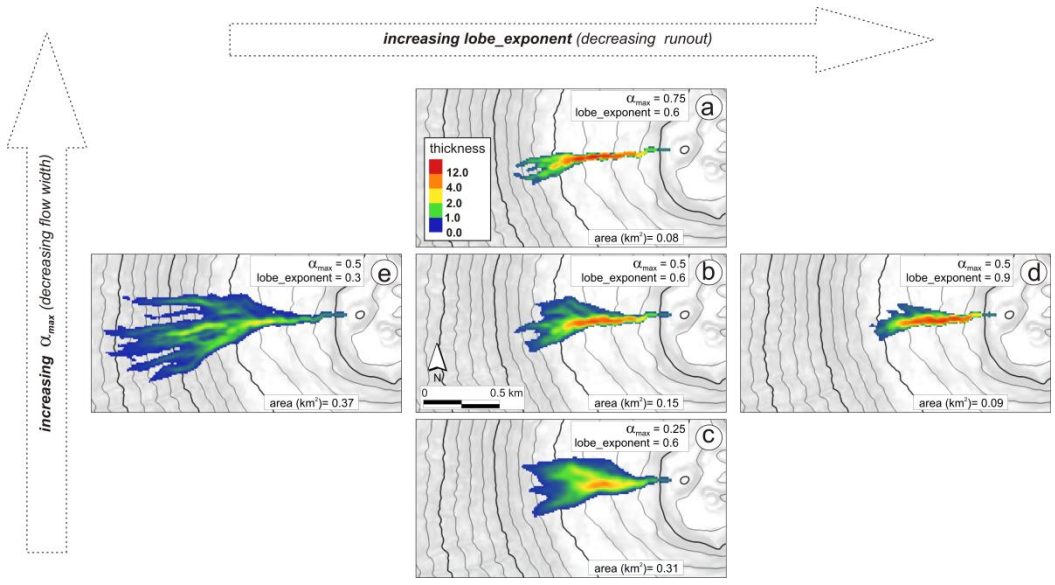

Figure 8. Masked grids of the thickness (for 156300 lava parcels) illustrating how the output of MrLavaLoba simulations change as the main input parameters *max_slope_prob* and *lobe_exponent* also change (all other factors remaining constant).

3.5. Accounting for the effect of syn-emplacement topographic changes

The key characteristic of MrLavaLoba, which marks a difference with respect to other probabilistic codes such as DOWNFLOW (Favalli et al. 2005), is the fact that computational parcels are assigned a volume. Users can choose to account or not for the modification of the topography due to the volume of the already emplaced parcels.

MrLavaLoba accounts for the modification of the topography through two specific settings: (i) the parameter *topo_mod_flag*, identifying how often the changes in topography are computed, and the parameter *thickening_parameter*, determining the weight assigned to these changes when computing the direction of propagation of new lobes. The more often changes are computed and the lower the *thickening_parameter* assigned (which can vary between 0 and 1), the higher the lateral spreading of the flow and the lower the thickness of the final lava deposit. It is important to highlight that even when changes in topography are considered during the emplacement, the outputs converge as shown in Figures 6-7. In general, this specific setting can be used to reproduce a given trend of supply rate (and consequent emplacement style) such as a continuous or episodic supply (Guest et al. 1987; Harris and Neri 2002).

3.6. The size of the parcel

Within a single simulation, all the parcels have the same area defined by the user as an input parameter. The optimal area of the parcel depends also on the cell size of the grid used as computational domain (i.e. the digital elevation model representing the topography). Considering computational lobes having an area smaller than the cell size of the computational grid does not improve the accuracy of simulations. In general, it is useful to keep the area of the parcel

as large as possible, without reducing the accuracy of the results (assessed on a case by case basis). By running the code preliminarily with a spectrum of different parcel sizes, it is usually easy to select the size which provides the optimal trade-off, because outputs obtained by considering exceedingly small or exceedingly large parcels produce too small or too large flow units, while the right size (i.e. the one similar to the real flow units) is missing. As a general rule, care should be made to choose a parcel size smaller than a characteristic width of typical flow units for a given scenario. As an example, in the case of channelized flow at Mt Etna considered in Figures 4, 5 and 8 (using a 10 m-cell size DEM – 100 m^2 cell area), we realized that there is a characteristic size of the features formed during the emplacement (e.g. characteristic dimension of the flow units), which are better reproduced by a parcel size of 1000-2000 m^2, while a significantly smaller parcel size produces narrower features which are negligible in real cases.

The parcel thickness is determined by the cumulative volume of the effusive episode in question, the parcel area and the total number of parcels. A higher number of parcels reduces the thickness and consequently the parcel volume. Thus, for a given cumulative lava volume, the computational time will increase proportionally to the number of parcels.

4. Using the code and case studies

MrLavaLoba has been written in Python and the source code is accessible at the code repository. Python is a widely used general-purpose, high-level programming language designed to emphasize code readability and conciseness (Oliphant 2007). Python interpreters are freely downloadable for installation on any operating system (e.g. Windows, Apple, Linux, Android), so that Python codes have great portability. Moreover, several GIS software such as Q-GIS, Grass and ArcGIS, provide a simple way to embed Python code in their GIS environment (Bartolini et al., 2013). It has been decided to release the code without embedding it in a specific GIS environment or interface for the following reasons: (i) to leave all future users free to load the simulation output

into their own GIS software; and (ii) to force future users to read the largely commented list of input settings, thus becoming a bit more familiar with the many nuances of MrLavaLoba.

The easiest way to become familiar with the code is to run it for a given scenario. To support this option, the test cases illustrated in the following can be downloaded from the code repository.

4.1. Input settings

As already highlighted, the code is structured to work with a large spectrum of input settings. In order to make tuning easier, we arranged input parameters into two input files: the first one ("input_data.py") collects basic settings such as type and coordinates of the vent(s), the size of the parcels, the cumulative volume of lava, the reference topography and all the very fundamental tuning parameters; the second input file ("input_data_advanced.py"), instead, includes secondary settings which can be tuned for a more advanced calibration, but can be left in their default values during the initial tuning. Examples of input files for the current version of MrLavaLoba are provided along with the source Python code. All the input parameters are listed and commented in detail to minimize misunderstandings.

4.2. Application to real cases

In this section, we present the application of MrLavaLoba to two real cases of lava flows emplaced according to very different dynamics at Hawaii and Mt Etna (i.e. pahoehoe and channelized-'a'ā, respectively).

4.2.1. The distal sector of the Kilauea 2014-2016 pahoehoe flow field

As a first test case, we considered the pahoehoe flow field which erupted at Kilauea volcano (Hawaii) between June 27, 2014 - June 8, 2015 (Patrick et al. 2016). On June 27, 2014, the opening of new vents on the north flank of Pu'u 'Ō'ō changed the hazard potential of ensuing lava flows dramatically, because lava advanced in a general northeast direction, posing a threat to the village of

549 Pahoa and other inhabited areas (Patrick et al. 2016). 7-8 km down-flow from
550 the vent, lavas repeatedly entered pre-existing ground cracks along the East Rift
551 Zone (ERZ), and continued to advance northeastwards for a few kilometers
552 (Figure 9a). In early September lava returned to the surface, heading in a more
553 northward direction, and continued advancing until March 2015. Given the
554 complexity of the whole episode, and the peculiar presence of the ground
555 cracks, mostly smaller the 20 m-cell size resolution of the topography used
556 here, we decided to simulate only the terminal segment, setting a
557 computational vent along the ERZ where lava exited from the ground cracks to
558 flow again on the surface (Figure 9b). In this case, our simulations were
559 supported by USGS colleagues based at the Hawaiian observatory, who
560 provided a pre-emplacement digital elevation model (a 20 m-resolution DEM
561 obtained from the 10 m-resolution NED topography, Gesch et al., 2002) and
562 lava coverage in addition to input settings such as an estimation of the volume
563 of lava flowed through the computational vent considered. Unfortunately, no
564 map of the thickness of the final lava deposit was available to validate the
565 simulation results with respect to the thickness.
566 Considering the complexity of the scenario and the relatively low quality
567 of the available DEM, the obtained result can be considered promising. Defining
568 a fitness index for the simulation as $\phi = (A_R \cap A_S)/(A_R \cup A_S)$, where A_R is the
569 area covered by the real flow and A_S the area covered by our simulation (Favalli
570 et al., 2009c), we obtain ϕ = 0.36. It is worthy to note that the masked output
571 shown in Figure 9b presents isolated pockets. This appears, of course,
572 unrealistic if we think about a real lava flow, but, when considered from a
573 probabilistic point of view, those pods represent areas more likely inundated
574 than the immediate surroundings.
575

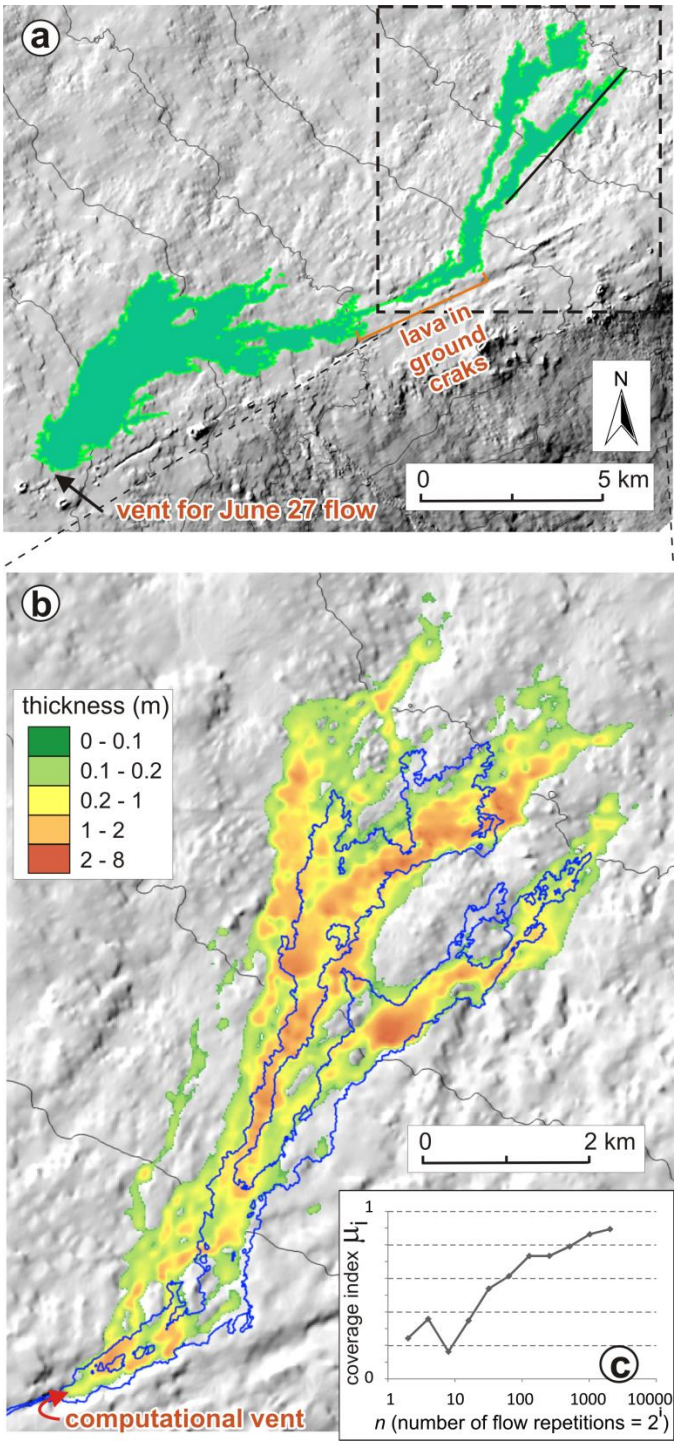

Figure 9. Simulation of the distal segment of the Kilauea 2014-2016 pahoehoe flow field. (a) map of the total flow field (after Patrick et al. 2016), contour lines are spaced at 100 m in elevation. (b) simulation result: masked grid of the thickness. (c) plot of the convergence for the selected input settings. The 20 m-cell size pre-emplacement topography is courtesy of M Patrick from USGS. Input parameters used as well as the DEM are accessible at the model repository.

4.2.2. The Mt Etna 2001 LFS1 lava flow

585 The second test case considered is the Mt Etna 2001 LFS1 flow field, which
586 formed from July 18 - August 9 2001 from a vent located at about 2100 m
587 elevation near Monti Calcarazzi (Coltelli et al. 2007). This flow is becoming a
588 kind of a benchmark for lava flow simulation codes, and has been simulated
589 repeatedly over the years with different codes (Crisci et al. 2004; Proietti et al.
590 2009; Tarquini and Favalli 2011; Mossoux et al. 2016). The cumulative volume
591 of lava emplaced is known from the existing literature (Coltelli et al. 2007), and
592 the map of the lava deposit thickness has been already presented by Tarquini
593 and Favalli (2011, Figure 10a). Here we used as pre-emplacement topography
594 the 10 m-resolution TINITALY digital elevation model (Tarquini et al. 2007;
595 2012b). The flow thickness for a simulation obtained with 2^{13} flow repetitions is
596 shown in Figure 10b. By comparing this coverage area for this particular run
597 with the real coverage, we have obtained a fitness index ϕ = 0.47. The
598 simulation tends to overestimate the inundated area. As for the obtained
599 thickness, in the first half of the flow the obtained thickness are consistently
600 low, and both the real and the simulated flow show a peak above 30 m at about
601 3 km from the vent. In the second half of the flow, instead, the mass
602 distribution is more distributed towards the front in the real case than in the
603 simulated one. Figure 10c shows the convergence of the simulation results in
604 terms of both area coverage and local thickness. Similarly to the Hawaiian case
605 presented in the previous section, both input data and DEM are provided as
606 supplementary material.
607

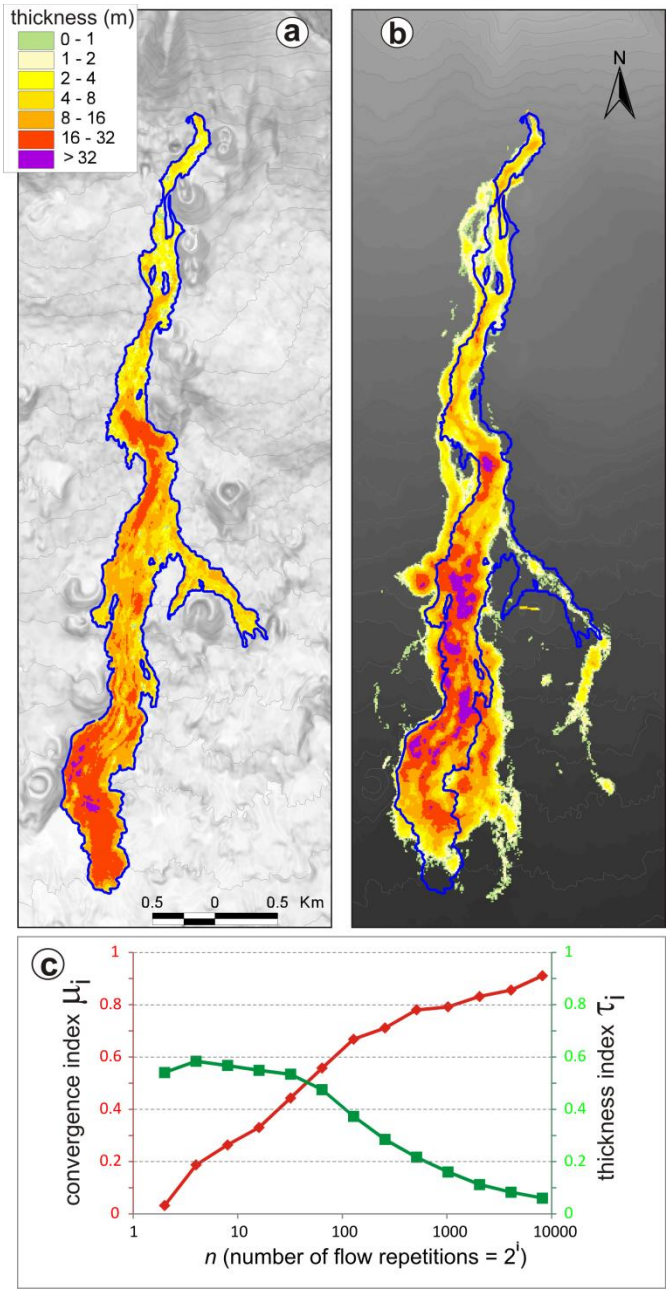

Figure 10. Simulation of the Mt Etna 2001 LFS1 ‘a‘ā flow field. (a) map of the thickness of the final flow field (obtained from DEM difference). (b) simulation results: masked grid of the thickness. (c) plot of the convergence for the selected input settings (for both coverage and thickness). The 10 m-cell size pre-emplacement topography is provided by INGV (Tarquini et al., 2012b). Input settings as well as the DEM are accessible at the code repository. The obtained fitness index for the simulation is $\phi = 0.47$. Time for a simulation on a standard PC is about 2’30’’ for the buddying of > 200,000 lobes having an area 10 times the cellsize of the computational DEM.

5. Discussion

The main principle at the foundation of MrLavaLoba is that uncertainty always affects the modeling of lava flows. This uncertainty is due both to the uncertainty of observations of critical input parameters such as the effusion rate (Harris et al. 2007) or the DEM, and to the extraordinary complexity in the emplacement processes of pahoehoe and ‘a‘ā lavas (Baloga and Glaze 2003; Applegarth et al. 2010a, 2010b; Favalli et al. 2010; James et al. 2012; Glaze and Baloga 2013). This concept has been largely validated for channelized flows by the success of the probabilistic code DOWNFLOW (Favalli et al. 2005, 2009, 2011, 2012), which embed a Monte Carlo approach consisting in the repetition of many, slightly perturbed steepest descent paths. A probabilistic approach is also followed by Glaze and Baloga (2013) in approaching the simulation of the emplacement of pahoehoe lavas. MrLavaLoba uses an approach similar to that of Glaze and Baloga (2013), with the scientific advancement of utilizing a stochastic perturbation of the main driving factor of lava flow emplacement (i.e. the steepest descent path), introducing a variety of tunable settings, and the probabilistic assessment of the convergence of the results.

In cellular automata models such as SCIARA (Crisci et al. 2010), changes to the pre-emplacement topography due to the emplacing lava is considered at each computational step. This appears to be a conservative choice. In contrast, previous probabilistic codes such as DOWNFLOW do not account at all for changes in the topography due to the emplacing lava. For short-lived or relatively simple flows, it is not necessary to account for changes in volume as often as is done in cellular automata codes to achieve realistic results (Tarquini and Favalli 2016). MrLavaLoba provides an intermediate solution in between these two extremes, and changes to the pre-emplacement topography determined by the volume of the emplacing lava flows can be calculated at a desired frequency by tuning specific parameters.

6. Conclusion

We have presented MrLavaLoba, a new code for the simulation of the area inundated by lava flows, freely downloadable at http://demichie.github.io/MrLavaLoba. MrLavaLoba is a probabilistic model that calculates the most probable areas that could be inundated by lava and the thickness of the deposits. The code does not provide directly the progression of a flow field with time. The code is written to be versatile. Input files provide tunable parameters that enable the generation of realistic results for a range of lava types and characteristics and for different emplacement dynamics. MrLavaLoba input parameters must be tuned for each new lava flow scenario based on an appropriate case. Upon proper parameters calibration, the code produces realistic results in different lava flow scenarios, from pahoehoe flows to channelized ‘a‘ā flows. Simulation results must be interpreted with the care due to the highly tunable and probabilistic nature of the model.

Acknowledgements

Many thanks goes to several colleagues at the Iceland Meteorological Office (Iceland, Esther Jensen, Melissa Pfeffer and Sara Barsotti), the United States Geological Survey (USA, Hannah Dietterich and Matthew Patrick), Stefania Bartolini and Gro Pedersen for help in testing the code and providing useful suggestions. ST acknowledges the ESF MeMoVolc Grant n. 6409, the EUFAR HOLUHRAUN_HAZ project and the Rannis EMMIRS project. Insightful reviews by two anonymous reviewers are gratefully acknowledged.

References

Applegarth LJ, Pinkerton H, James MR, Calvari S (2010a) Lava flow superposition: The reactivation of flow units in compound 'a'ā flows. J Volcanol Geotherm Res 194:100-106. doi:10.1016/j.jvolgeores.2010.05.001

Applegarth LJ, Pinkerton H, James MR, Calvari S (2010b) Morphological complexities and hazards during the emplacement of channel-fed `a`ā lava flow fields: a study of the 2001 lower flow field on Etna. Bull Volcanol 72:641–656, http://dx.doi.org/10.1007/s00445-010-0351-1

Baloga SM, Glaze LS (2003) Pahoehoe transport as a correlated random walk. J Geophys Res 108(B1). doi:10.1029/2001JB001739

Bartolini S, Cappello A, Martí J, Del Negro C (2013) QVAST: a new Quantum GIS plugin for estimating volcanic susceptibility. Nat. Hazards Earth Syst Sci 13:3031–3042. doi:10.5194/nhess-13-3031-2013

Behncke B, Neri M, (2003) The July–August 2001 eruption of Mt. Etna (Sicily). Bull Volcanol 65, 461–476. doi:10.1007/s00445-003-0274-1

689 Behncke B, Neri M, Carniel R (2003) An exceptional case of endogenous lava dome growth
690 spawning pyroclastic avalanches: the 1999 Bocca Nuova eruption of Mt. Etna (Italy). J
691 Volcanol Geotherm Res 124:115–128
692 Borgia A, Linneman S, Spencer D, Diego Morales L, Brenes Andres J (1983) Dynamics of lava flow
693 fronts, Arenal Volcano, Costa Rica. J Volcanol Geotherm Res 19:303–329
694 Calvari S, Pinkerton H (2002) Instabilities in the summit region of Mount Etna during the 1999
695 eruption. Bull Volcanol 63:526–535
696 Calvari, S., Neri, M., Pinkerton, H., 2002. Effusion rate estimations during the 1999 summit
697 eruption on Mount Etna, and growth of two distinct lava flow fields. J Volcanol Geotherm
698 Res 119:107–123
699 Cappello A, Ganci G, Calvari S, Pérez NM, Hernández PA, Silva SV, Cabral J, Del Negro C (2016)
700 Lava flow hazard modeling during the 2014–2015 Fogo eruption, Cape Verde. Journal of
701 Geophysical Research: Solid Earth 121, 2290-2303
702 Castruccio A, Rust AC, Sparks RSJ (2014) Assessing lava flow evolution from post-eruption field
703 data using Herschel-Bulkley rheology. J Volcanol Geotherm Res 275:71-84
704 Chopin N. (2011) Fast simulation of truncated Gaussian distributions. Statistics and Computing
705 21, https://arxiv.org/pdf/1201.6140.pdf
706 Crisci, G., R. Rongo, S. Di Gregorio, and W. Spataro (2004), The simulation model SCIARA: The
707 1991 and 2001 lava flows at Mount Etna, J. Volcanol. Geotherm. Res., 132, 253–267,
708 doi:10.1016/S0377-0273(03)00349-4.
709 Crisci, G.M., Avolio, M.V., Behncke, B., D'Ambrosio, D., Di Gregorio, S., Lupiano, V., Neri, M.,
710 Rongo, R., Spataro, W., 2010. Predicting the impact of lava flows at Mount Etna, Italy.
711 Journal of Geophysical Research 115, B04203. http://dx.doi.org/10.1029/2009JB006431.
712 Cordonnier B, Lev E, Garel F (2016) Benchmarking lava-flow models. Geological Society, London,
713 Special Publications 426 (1), 425-445
714 Del Negro, C., L. Fortuna, A. Herault, and A. Vicari (2008), Simulations of the 2004 lava flow at
715 Etna volcano by the MAGFLOW cellular automata model, Bull. Volcanol., 70, 805–812,
716 doi:10.1007/s00445-007-0168-8.
717 Dietterich HR, Cashman KV (2014) Channel networks within lava flows: Formation, evolution,
718 and implications for flow behavior. Journal of Geophysical Research: Earth Surface 119 (8),
719 1704-1724
720 Dietterich HR; Lev E; Chen J; Richardson JA; Cashman KV (2017) Benchmarking computational
721 fluid dynamics models of lava flow simulation for hazard assessment, forecasting, and risk
722 management. J Applied Volcanol 6:9 DOI 10.1186/s13617-017-0061-x
723 Favalli, M., Pareschi, M.T., Neri, A., and Isola, I., 2005, Forecasting lava fl paths by a stochastic
724 approach: Geophys Res Lett 32:L03305, doi: 10.1029/2004GL021718.
725 Favalli M., Tarquini S., Fornaciai A., Boschi E. (2009a). A new approach to risk assessment of lava
726 flow at Mount Etna. Geology 37:1111-1114. doi:10.1130/G30187A
727 Favalli M, Mazzarini F, Pareschi MT, Boschi E (2009b) Topographic control on lava flow paths at
728 Mt. Etna (Italy): implications for hazard assessment J Geophys Res 114:F01019.
729 doi:10.1029/2007JF000918
730 Favalli, M., F. Mazzarini, M. T. Pareschi, and E. Boschi (2009c) Topographic control on lava flow
731 paths at Mount Etna, Italy: Implications for hazard assessment, J. Geophys. Res., 114,
732 F01019, doi:10.1029/2007JF000918
733 Favalli M., Fornaciai A., Mazzarini F., Harris A.J.L., Neri M., Behncke B., Pareschi M. T., Tarquini
734 S., Boschi E. (2010). Evolution of an active lava flow field using a multitemporal LIDAR
735 acquisition, J Geophys Res 115:B11203. doi:10.1029/2010JB007463
736 Favalli, M., Tarquini, S., Fornaciai, A., 2011. DOWNFLOW code and Lidar technology for lava flow
737 analysis and hazard assessment at Mount Etna. Ann Geophys-Italy 54:552–566.
738 http://dx.doi.org/10.4401/ag-5339.
739 Favalli M., Tarquini S., Papale P., Fornaciai A., Boschi E. (2012). Lava flow hazard and risk at Mt.
740 Cameroon volcano. Bulletin of Volcanology 74, 423-439. doi:10.1007/s00445-011-0540-6.
741 Felpeto A, Arana V, Ortiz R, Astiz M, Garcia A (2001) Assessment and modelling of lava flow
742 hazard on Lanzarote (Canary Islands). Nat Hazards 23:247–257
743 Frazzetta G, Romano R (1984) The 1983 Etna eruption: event chronology and morphological
744 evolution of the lava flow. Bull Volcanol 47:1079–1096
745 Gesch, D., Oimoen, M., Greenlee, S., Nelson, C., Steuck, M., Tyler, D., 2002. The National
746 Elevation Dataset. ISPRS J. Photogramm. Remote. Sens. 68, 5–32.

747 Giacomini L, Massironi M, Martellato E, Pasquarè G, Frigeri A, Cremonese G (2009) Inflated
748 flows on Daedalia Planum (Mars)? Clues from a comparative analysis with the Payen
749 volcanic complex (Argentina). Planet Space Sci 57:556-570. doi:10.1016/j.pss.2008.12.001.
750 Gilbert JS, Sparks RSJ (1998) Future research directions on the physics of explosive volcanic
751 eruptions. In: Gilbert JS & Sparks RSJ (eds) The Physics of Explosive Volcanic Eruptions.
752 Geological Society, London, Special Publications, 145, 1-7
753 Glaze LS, Baloga SM (2006) Rheologic inferences from the levees of lava flows on Mars, J.
754 Geophys. Res., 111, E09006, doi:10.1029/2005JE002585
755 Glaze LS, Baloga SM (2013) Simulation of inflated pahoehoe lava flows. J Volcanol Geotherm Res
756 255:108–123. doi:10.1016/j.jvolgeores.2013.01.018
757 Glaze, L. S., S. M. Baloga, W. B. Garry, S. A. Fagents, and C. Parcheta (2009), A hybrid model for
758 leveed lava flows: Implications for eruption styles on Mars. J Geophys Res 114:E07001,
759 doi:10.1029/2008JE003278
760 Guest JE, Kilburn CRJ, Pinkerton H, Duncan AM (1987) The evolution of lava flow-fields:
761 observations of the 1981 and 1983 eruptions of Mount Etna, Sicily. Bull Volcanol 49:527–
762 540
763 Hamilton CW, Glaze LS, James MR, Baloga SM (2013) Topographic and stochastic influences on
764 pāhoehoe lava lobe emplacement. Bull Volcanol 75: 756. doi 10.1007/s00445-013-0756-8.
765 Harris AJL, Rowland SK (2001) FLOWGO: a kinematic thermo-rheological model for lava flowing
766 in a channel. Bull Volcanol 63:20–44
767 Harris AJL, Neri M (2002) Volumetric observations during paroxysmal eruptions at Mount Etna:
768 pressurized drainage of a shallow chamber or pulsed supply? J Volcanol Geotherm Res
769 116:79–95
770 Harris AJL, Flynn LP, Matías O, Rose WI (2002) The thermal stealth flows of Santiaguito:
771 implications for the cooling and emplacement of dacitic block lava flows. Geol Soc Am Bull
772 114:533–54
773 Harris AJL, J Dehn, S Calvari (2007) Lava effusion rate definition and measurement: a review.
774 Bull Volcanol 70:1–22. doi:10.1007/s00445-007-0120-y
775 Harris AJL, Rowland SK (2009). Effusion rate controls on lava flow length and the role of heat
776 loss: a review. In: Thordarson, T., Self, S., Larsen, G., Rowland, S.K., Hoskuldsson, A. (Eds.),
777 Studies in Volcanology: The Legacy of George Walker: Special Publication IAVCEI, 2, pp. 33–
778 51
779 Harris AJL, Carn S, Dehn J, Del Negro C, Guđmundsson MT, ... (2016) Conclusion:
780 recommendations and findings of the RED SEED working group. In: Harris AJL, De Groeve T,
781 Garel F, Carn SA (eds) Detecting, Modelling and Responding to Effusive Eruptions.
782 Geological Society, London, Special Publications, 426. http://doi.org/10.1144/SP426.11
783 Hidaka, M., A. Goto, S. Umino, and E. Fujita (2005), VTFS project: Development of the lava flow
784 simulation code LavaSIM with a model for three-dimensional convection, spreading, and
785 solidification, Geochem. Geophys. Geosyst., 6, Q07008, doi:10.1029/2004GC000869
786 Hoblitt RP, Orr TR, Heliker C, Denlinger RP, Hon K, Cervelli PF (2012) Inflation rates, rifts, and
787 bands in a pāhoehoe sheet flow. Geosphere 8(5):179–195. doi:10.1130/GES00656.1
788 Hon K, Kauahikaua J, Denlinger R, Mackay K (1994) Emplacement and inflation of pahoehoe
789 sheet flows: Observations and measurements of active lava flows on Kilauea Volcano,
790 Hawaii. Geol Soc Am Bull 3:351-370
791 Kauahikaua J, Cashman KV, Mattox TN, Heliker CC, Hon KA, Mangan MT, Thornber CR (1998)
792 Observations on basaltic lava streams in tubes from Kilauea Volcano, island of Hawai'i. J
793 Geophys Res 103 B11:27,303-27,323
794 Kilburn CRJ (2000) Lava Flows and Flow Fields. In: Sigurdsson, H. (Ed.), Encyclopedia of
795 Volcanoes. Academic Press, San Diego, CA, pp. 291-306
796 Kilburn CRJ, Lopes RMC (1988) The growth of aa lava flow fields at Mount Etna. Sicily. J Geophys
797 Res 93 (B12):14759–14772.
798 Kilburn CRJ, Lopes RMC (1991) General patterns of flow field growth: Aa and blocky lavas.
799 Journal of Geophysical Research: Solid Earth 96 (B12), 19721-19732
800 James MR, Pinkerton H, Robson S (2007) Image based measurement of flux variation in distal
801 regions of active lava flows. Geochem Geophys Geosyst 8, Q03006.
802 doi:10.1029/2006GC001448

James MR, Pinkerton H, Applegarth LJ (2009) Detecting the development of active lava flow fields with a very-long-range terrestrial laser scanner and thermal imagery. Geophys. Res. Lett., 36, L22305, doi:10.1029/2009GL040701.

James MR, Applegarth LJ, Pinkerton H (2012) Lava channel roofing, overflows, breaches and switching: insights from the 2008–2009 eruption of Mt. Etna. Bull Volcanol 74:107-117

Jurado-Chichay Z, Rowland SK (1995) Channel overflows of the Pohue Bay flow, Mauna Loa, Hawaii: examples of the contrast between surface and interior lava. Bull Volcanol 57 :117–126

Lipman PW, Banks NG (1987) Aa flow dynamics, Mauna Loa. In: Decker W, Wright TL, Stauffer PH (eds) Volcanism in Hawaii. US Geol Surv Prof Paper no. 1350, pp 1527–1567

Macedonio, G., M. T. Pareschi, and R. Santacroce (1990), A simple model for lava hazard assessment: Mount Etna, paper presented at International Volcanological Congress, Int. Assoc. of Volcanol. and Chem. of the Earth's Inter., Mainz, Germany, Sept.

Miyamoto H, Papp KR (2004) Rheology and topography control the path of a lava flow: insight from numerical simulations over a preexisting topography. Geophys Res Lett 31:L166085. doi:10.1029/2004GL020626

Mossoux S, Saey M, Bartolini S, Poppe S, Canters F, Kervyn M (2016) Q-LAVHA: A flexible GIS plugin to simulate lava flows. Computers & Geosciences 97, 98-109

Oliphant TE (2007) Python for Scientific Computing. Computing in Science and Engineering 9:10-20. DOI: 10.1109/MCSE.2007.58

Patrick M, Orr T, Fisher G, Trusdell F, Kauahikaua J (2016) Thermal mapping of a pāhoehoe lava flow, Kīlauea Volcano. J Volcanol Geotherm Res http://dx.doi.org/10.1016/j.jvolgeores.2016.12.007

Pedersen GBM, Höskuldsson A, Dürig T, Thordarson T, Jónsdóttir I, Riishuus MS, Óskarsson BV, Dumont S, Magnusson E, Gudmundsson MT, Sigmundsson F, Drouin VJPB, Gallagher C, Askew R, Guðnason J, Moreland WM, Nikkola P, Reynolds HI, Schmith J (2017) Lava field evolution and emplacement dynamics of the 2014–2015 basaltic fissure eruption at Holuhraun, Iceland. J Volcanol Geotherm Res

Proietti C, Coltelli M, Marsella M, Fujita E (2009) A quantitative approach for evaluating lava flow simulation reliability: LavaSIM code applied to the 2001 Etna eruption. Geochemistry, Geophysics, Geosystems 10.

Richter N, Favalli M, de Zeeuw-van Dalfsen E, Fornaciai A, da Silva Fernandes RN, Perez Rodriguez N, Levy J, Silva Victória S, Walter TR (2016) Lava flow hazard at Fogo Volcano, Cape Verde, before and after the 2014-2015 eruption. Nat Hazards Earth Syst Sci Discuss doi:10.5194/nhess-2016-81

Self S, Keszthelyi L, Thordarson T (1998) The importance of pahoehoe. Annu Rev Earth Planet Sci 26:81-110

Tarquini S (2017) A review of mass and energy flow through a lava flow system: Insights provided from a non-equilibrium perspective. Bull Volcanol. DOI: 10.1007/s00445-017-1145-5

Tarquini S, de' Michieli Vitturi M (2014) Influence of fluctuating supply on the emplacement dynamics of channelized lava flows. Bull Volcanol 76: 801. doi:10.1007/s00445-014-0801-2.

Tarquini S, Favalli M (2010) Changes of the susceptibility to lava flow invasion induced by morphological modifications of an active volcano: the case of Mount Etna, Italy. Nat Hazards 54:537-546. doi:10.1007/s11069-009-9484-y.

Tarquini S, Favalli M (2011) Mapping and DOWNFLOW simulation of recent lava flow fields at Mount Etna. J Volcanol Geotherm Res 204, 27-39. doi:10.1016/j.jvolgeores.2011.05.001.

Tarquini S, Favalli M (2013) Uncertainties in lava flow hazard maps derived from numerical simulations: the case study of Mount Etna. J Volcanol Geotherm Res 260, 90-102. doi:10.1016/j.jvolgeores.2013.04.017

Tarquini S, Favalli M (2016) Simulating the area covered by lava flows using the DOWNFLOW code. In: Harris AJL, De Groeve T, Garel F, Carn SA (eds) Detecting, Modelling and Responding to Effusive Eruptions. Geological Society, London, Special Publications, 426. http://doi.org/10.1144/SP426.15

Tarquini S, Isola I, Favalli M, Mazzarini F, Bisson M, Pareschi MT, Boschi E (2007) TINITALY/01: a new Triangular Irregular Network of Italy. Annals of Geophysics 50, 407 - 425

Tarquini S, Favalli M, Mazzarini F, Isola I, Fornaciai A (2012a) Morphometric analysis of lava flow units: case study over LIDAR-derived topography at Mount Etna, Italy. J Volcanol Geotherm Res 235-236, 11-22. doi: 10.1016/j.jvolgeores.2012.04.026

Tarquini S., Vinci, S., Favalli M., Doumaz, F., Fornaciai A., Nannipieri, L. (2012b). Release of a 10-m-resolution DEM for the Italian territory: Comparison with global-coverage DEMs and anaglyph-mode exploration via the web. Computers & Geosciences 38, 168-170. doi:10.1016/j.cageo.2011.04.018

Thordarson T, Self S (1998) The Roza Member, Columbia River Basalt Group: A gigantic pahoehoe lava flow field formed by endogenous processes? J Geophys Res 103 Bll:27,411-27,445

Vicari, A., Ganci, G., Behncke, B., Cappello, A., Neri,M., Del Negro, C., 2011. Near-real-time forecasting of lava flow hazards during the 12–13 January 2011 Etna eruption. Geophysical Research Letters 38, L13317. http://dx.doi.org/10.1029/2011GL047545.

Wadge G (1978) Effusion rate and the shape of aa lava flow-fields on Mt Etna. Geology 6:503-506

Wadge G (1981) The variation of magma discharge during basaltic eruptions. J Volcanol Geotherm Res 11:139-168

Wadge G, Saunders S, Itikarai I (2012) Pulsatory andesite lava flow at Bagana Volcano. Geochem Geophys Geosyst 13:Q11011. doi:10.1029/2012GC004336

Walker GPL (1971) Compound and simple lava flows and flood basalts. Bull Volcanol 35:579–590

Walker GPL (1973) Lengths of lava flows. Phil Trans Roy Soc London A—Math Phys and Eng Sci 274:107–118

Walker GPL (1991) Structure, and origin by injection under surface crust, of tumuli, “lava rises”, “lava-rise pits” and “lava inflation clefts” in Hawaii. Bull Volcanol 53:546-558

Walker GPL (2009) The endogenous growth of pahoehoe lava lobes and morphology of lava-rise edges. In: Thordarson, T., Self, S., Larsen, G., Rowland, S.K., Hoskuldsson, A. (Eds.), Studies in Volcanology: The Legacy of George Walker. Special Publications of IAVCEI, 2. Geological Society, London, pp. 17–32.

Wantim MN, Kervyn M, Ernst GGJ, del Marmol MA, Suh CE, Jacobs P (2013) Numerical experiments on the dynamics of channelised lava flows at Mount Cameroon volcano with the FLOWGO thermo-rheological model. J Volcanol Geotherm Res 253, 35-53

Wright, R., Garbeil, H., Harris, A.J.L., 2008. Using infrared satellite data to drive a thermorheological/stochastic lava flow emplacement model: a method for near-real-time volcanic hazard assessment. Geophys. Res. Lett. 35, L19307. http://dx.doi.org/10.1029/2008GL035228.

Young P, Wadge G (1990) FLOWFRONT: simulation of a lava flow. Computers & Geosciences 16: 1171-1191. doi:10.1016/0098-3004(90)90055-X